



## Synthesizing a massive training dataset based on real lunar data for image-based navigation and crater recognition

*Hoonhee Lee*

*Korea Aerospace Research Institute (KARI)  
169-84 Gwahak-ro, Yuseong-gu, Daejeon 34133, South Korea  
lhh@kari.re.kr*

*Dawoon Jung*

*Korea Aerospace Research Institute (KARI)*

*Seunghee Son*

*Korea Aerospace Research Institute (KARI)*

*Han-Lim Choi*

*Korea Advanced Institute of Science and Technology (KAIST)*

### ABSTRACT

Image-based navigation is a key technology for landing on the Moon and other planetary bodies. Image-based navigation requires real-time crater detection/recognition for position determination during descent and touchdown. In this research, we present an algorithm that uses lunar images to assist in navigation and/or landing. In particular, this algorithm is able to robustly recognize craters in sub-optimal illumination conditions such as near the lunar South Pole where permanently shadowed regions exist. Until now, image-based crater recognition and counting algorithms required well-lit, clearly-defined features. The proposed algorithm utilizes a machine-learning technique known as a convolutional neural network (CNN). This approach requires an extensive training set to successfully classify and recognize images. We propose generating CNN training data using synthetic lunar images based on digital elevation models (DEMs). Since the Moon has no atmosphere, its surface does not substantially change over time ensuring that computer-generated images will closely resemble ground truth. Several tens of thousands of images are rendered with differing camera parameters and Sun positions. The algorithm was tested by training the CNN on generated images of the Shackleton, de Gerlache and Shoemaker craters. The trained CNN is confirmed to recognize these craters in real lunar images with a high degree of accuracy. In summary, this research presents a novel method of generating and using synthetic lunar images for assisting in the navigation of spacecraft or landers. The method was tested by generating images of craters near the South Pole under varying viewing and illumination conditions, training a CNN with the generated images, and verifying that the CNN recognizes the trained craters accurately. This technique is robust under challenging illumination conditions and is suitable for navigation near the lunar South Pole.

**KEYWORDS** : *CNN, ConvNets, Convolutional Neural Network, Image based Navigation*

### NOMENCLATURE

$\Theta_1$  - Elevation angle from centre of crater to the Sun  
 $\phi_1$  - Azimuth angle from the North to the Sun, clockwise around crater horizon  
 $\Theta_2$  - Elevation angle from center of crater to camera  
 $\Phi_2$  - Azimuth angle from the North to the camera, clockwise around crater horizon  
 $\sigma$  - Ratio of width of square to a crater diameter  
 $\alpha$  - Diameter of crater



- **INTRODUCTION**

The Korean lunar exploration program started in January 2016 and is currently in the preliminary design phase of a lunar orbiter that will carry a variety of scientific payloads including optical cameras. Research and development of key technologies for a future lander and surface rover is also taking place. Candidate landing sites might include maria or rugged highlands. In particular, the lunar poles, which have a high probability of harbouring reserves of water, are particularly interesting yet challenging destinations for lander missions.

In this study, we propose a machine learning method for lunar navigation in polar regions that is capable of high performance even with very limited training data.

At the Moon and Mars, where satellite-based accurate position information cannot be obtained, the current position, attitude, or velocity is calculated by referencing topography or other surrounding features. Previous studies have focused on flat landing sites with clearly-discernible terrain such as lunar maria at equatorial latitudes. For example, algorithm [1] finds the centre and size of a circular or elliptical crater on flat terrain, and matches it with an existing database of craters or generates navigation parameters relative to surrounding craters. This method is difficult to use in high-latitude regions however because of low Sun elevation angles that cause elongation and truncation of apparent crater outlines due to shadowing.

Instead of considering shadows as obstacles to successful pattern matching, Shadow-Based Matching [2] uses shadows themselves as feature points or indicators for self-localization of a lunar lander. However, this method is unsuitable at polar latitudes where the majority of terrain is covered with overlapping shadows.

Support Vector Machine (SVM) [3] was used to classify image features as non-craters and craters [4]. However, only a small number of real images were used for training the network and results depend heavily on the preprocessing method used as opposed to Convolutional Neural Networks (CNN) [5]. In order to improve the performance of classical SVM, there is a recent case [6] in which CNN is applied to automatically search Mars topography. However this research did not try to recognize and identify single feature points or indicators, but to determine the distribution of features in a large area. CNN has also been applied in the case of the Moon [7], [8], but none of these address how to detect and classify irregular features, or to increase the amount of useful training data along trajectories that a lander might travel but no orbiter has taken.

The lack of training data is a common problem in machine learning algorithms, especially when the number of neural networks increases. A simple method to increase the volume of training data is to duplicate the original image and apply rotation, cropping, jittering, and mirroring [9]. However, the quantitative increase is limited and may not be applicable depending on the problem domain.

Instead of altering existing data, synthetic, labelled training data can be generated and has been applied to human gaze estimation [10]. However, this method concentrated on refining synthetic imagery and was applied in an environment where real images can be obtained sufficiently and has not been tested on terrain imagery.

DEM-based synthetic images combined with PCA and a polynomial classifier were used to recognize lunar craters [11]. However, the method was not tested on heavily-shadowed terrain. We expect that it is not suitable for polar navigation because of the high-dimensionality of complex, shadowed crater features.

In this paper, we present a CNN design and novel learning method that can perform effectively in dark, shadowed terrain such as the lunar poles. Section 2 presents background and motivation. Section 3 describes our method. Section 4 compares the performance of our LunarNet CNN with its feature based SVM according to parameter's changes. Finally, Section 5 discusses the results and directions for further research.

- **MOTIVATION**

DEM data acquired using the laser altimeters on board previous and current orbital missions forms the basis for constructing synthetic training images in this study. In the case of the Moon, the cost of producing each synthetic image is low because the surface remains fairly constant due to lack of weathering and so DEMs do not need to be updated frequently. Additionally, it is only necessary to

generate training images of the regions that will be visible along the mission trajectory which may be quite narrow for a lander.

As DEM data is acquired through active laser imaging, it provides accurate base geometry even in heavily-shadowed regions. However, we still need images that appear as they might be taken by a navigation camera; that is, correctly lit by sunlight. This can be achieved by generating, or rendering, scenes in simulation software taking as input the DEM, Sun position, camera trajectory and attitude, and field-of-view (FOV), and a surface reflectance model.

Fig. 1 shows a test rendering using LRO LROC LOLA [12] data compared with the corresponding real image taken by the Selenological and Engineering Explorer (SELENE [13]) High-Definition Television (HDTV) camera. A simplified Hapke reflectance model with five parameters was used. Shadows are approximated with shadow mapping [14] instead of more accurate ray tracing techniques. Differences from the real image such as the sharpness of shadow edges are due to use of these simplified light transport models. However, overall the synthetic image closely approximates the real image. This is because the Moon has no atmosphere and the topography of the pictured area is relatively smooth.

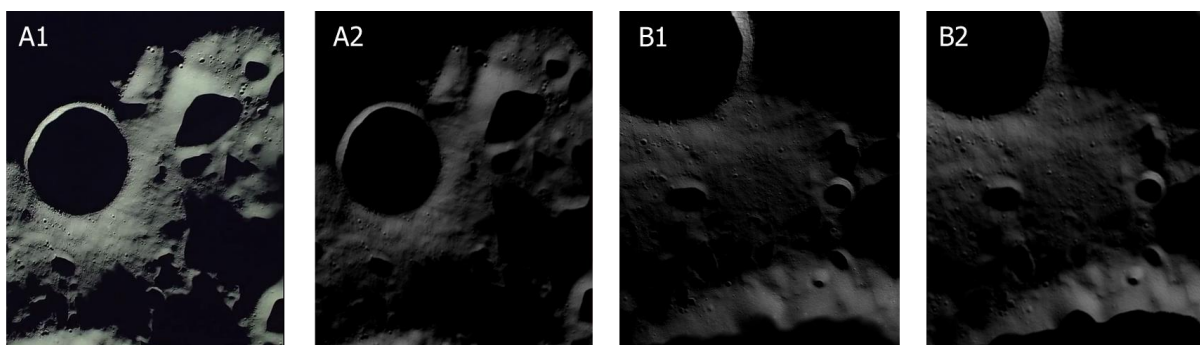


**Figure 1: Comparison between real images A1, B1 and synthetic images A2, B2 respectively (A1: a snapshot from SELENE HDTV, B1: DTMTCO\_03\_04806S893E0519PS from SELENE Terrain Camera)**

Additional training images can also be produced by photographing a physical scale model using a setup such as Fig. 2. These can be used in edge cases where purely-synthetic computer-renderings do not produce the desired result.



**Figure 2: Illuminated Hybrid Hardware-Software Simulation Bench at KARI [15]**

This paper makes the following contributions:

- We show that by changing the parameters for generating the synthetic image, the machine learning performance can be improved.
- We solve the data augmentation problem in machine learning by using a combination of real imagery, synthetic imagery, and DEM data in a feedback loop until performance is satisfied.
- We avoid overfitting and reduce the difference between the actual images and the model because we do not include actual images in the training data.

- **METHOD**
- **Machine-Learning System Overview**

Fig. 3 illustrates the novel machine learning system constructed for this paper. It is a closed-loop crater classifier that provides image-based navigation information suitable for dark polar regions characterised by heavy shadowing and lack of reliable training images.

The main features are described below.

1. In order to train the crater classifier to recognize craters (one feature of the terrain), the training set and validation set are generated from DEM-based synthetic rendered images only.
2. Real images obtained from actual lunar missions are used only to evaluate the performance of the crater classifier.
3. If the performance result does not meet the desired criteria, the system repeatedly changes image generation parameters to generate additional training and validation sets, and repeats the learning process. In general machine learning systems, the validation set is used to determine when to terminate learning but in this study, closed-loop learning can be performed indefinitely based on the threshold set by the user. However, since there will always be a small difference between model and reality, this threshold is assumed to be a trade-off target and the performance is assumed to converge at a certain value.

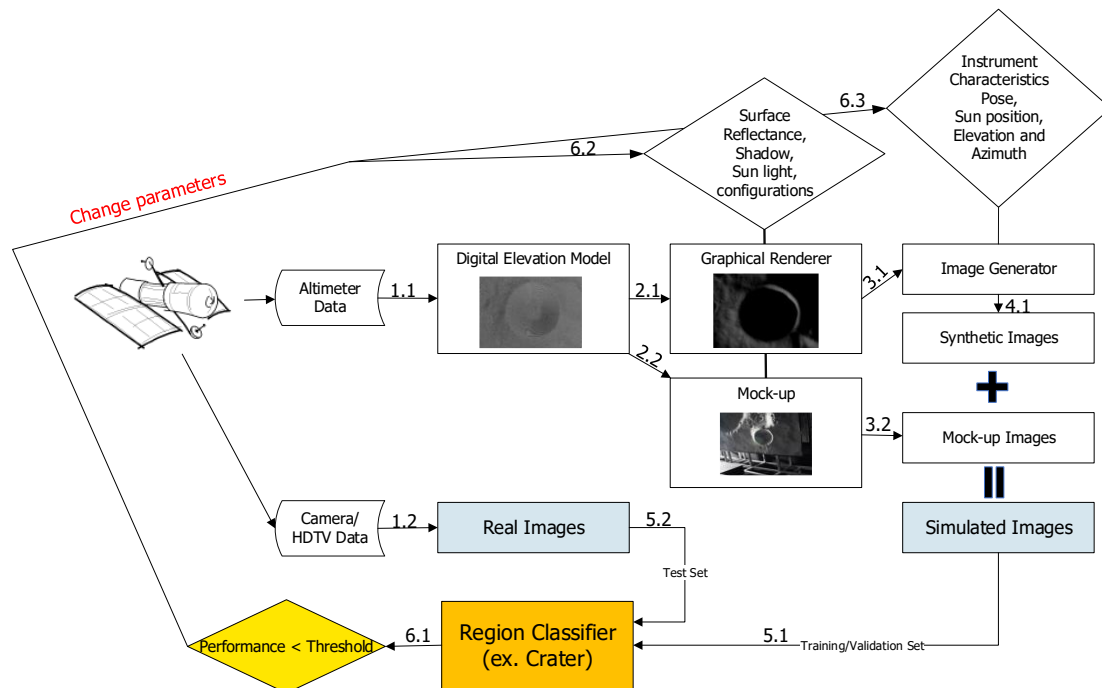


**Figure 3: Overall Training System basing Synthetic Images**

The purpose of (1) and (2) is to utilize synthetic images only for the training and validation sets, not the test set to avoid overfitting, assuming that the DEM-based synthetic images are similar to image obtained from actual cameras. (3) aims to optimize the learning process.

The mock-up in Fig. 3 was previously shown in Fig. 2. It is a test bench for simulating lander movement in three axes with the ability to photograph a lunar surface model under realistic illumination conditions. In this study, only synthetic images were used.

For this training system, we collected actual images of three craters, de Gerlache, Shackleton, and Shoemaker near the lunar South Pole and performed labelling to express the truth of each image. In addition, a high-resolution LOLA DEM was imported as a surface model using the method described in [16]. The synthetic image generation system takes as input the camera position, attitude, Sun position, and camera characteristics.

• **Test Configuration**

The DEM was based on data from the LRO Lunar Orbiter Laser Altimeter (LOLA) payload, currently the most accurate available at the lunar poles. Crater images were extracted from SELENE Terrain Camera (TC) and HDTV video frames, and LRO LROC images were also used. 3D images were created using the graphical renderer, PANGU [17], and the composite image was generated by changing the camera posture, position, and sun position of the lunar lander. The Sun was assumed to be monochromatic (white) and the lunar surface reflectance model was set to Hapke (a simplified version using five parameters and single wavelength). The crater classifier uses a high performance SVM as a non-neural network and a CNN with a shallow network for comparison. In the case of the SVM, the preprocessing performance of the feature is a very important factor. Therefore, we compare the results of the CNN and the optimal SVM by using feature that was created using the CNN.

**Table 1: Training Preparation**

Synthetic Images		Real Images		Crater Classifier	
Based DEM: LRO LOLA	de Gerlache (22,500 pics)	Image sources: 1. SELENE TC 2. HDTV, 3. LRO LROC	de Gerlache (300 pics)	Non-CNN : a multiclass SVM (CNN [LunarNet_ex] FC feature)	LunarSvm_ex
Graphical Renderer: PANGU	Shackleton (22,500 pics)		Shackleton (300 pics)		
	Shoemaker (22,500 pics)		Shoemaker (300 pics)	a shallow CNN	LunarNet_ex

From a camera and lunar surface perspective, both the sun and the camera have elevations and azimuth angles of 360 degrees. At the lunar South Pole, the elevation of the sun is actually within 1.6 degrees, and the image information taken below 1 degree is very small, so the range between 0.6 and 1.6 degrees is chosen. The elevation of the camera ranged from 54 to 90 degrees because it was insignificant in the testing phase because there was almost no lunar South Pole imagery taken at low elevation.

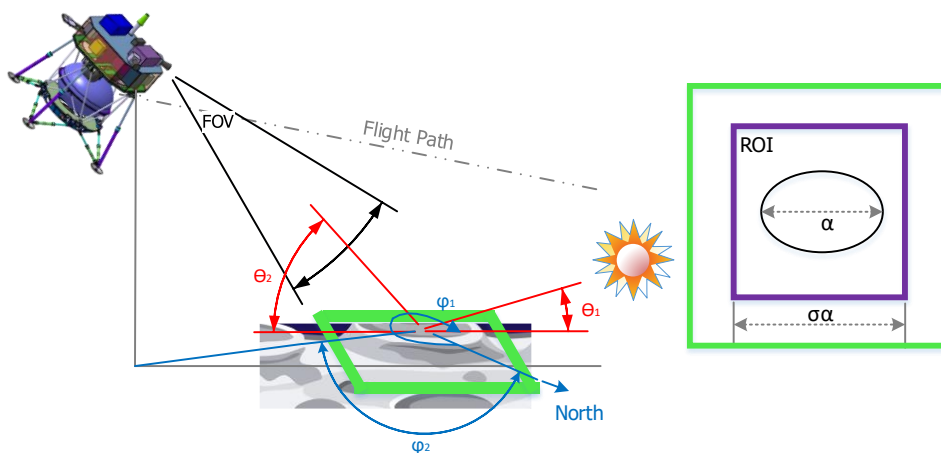


**Figure 4: Camera Pose Parameters**

The parameters for the generation of composite images are defined in detail. The position of the sun in Fig. 4 defines the angle azimuth  $\varphi_1$  between the axis of the sun toward the north of the Moon and the azimuth of the sun on the horizontal plane from the origin of the crater, and the elevation  $\Theta_1$  from the surface. The field of view (FOV) for the camera, the angle between the vertical axis and the focal axis of the camera at the centre of the crater  $\Theta_2$ , and azimuth  $\varphi_2$  are defined. The Purple box is the Region of Interest (ROI) that you want to use for learning in a wide 2D image (Green box) shot at 90 degrees FOV. In other words, the size of the ROI representing this learning range was considered as one parameter in this study. The ROI is a square and the ratio  $\sigma$  to the diameter  $\alpha$  of the crater's major axis is used to select the length of one side. For example, if  $\sigma$  is 1, the ROI becomes a square with the length of the major axis of the crater. The larger the ratio  $\sigma$ , the more pixel information around the crater is included.

Table 2: Parameters for Synthesis

Class	Parameter	Range	Sampling Frequency	Sampling Location
Sun	Elevation, $\Theta_1$	0.16 ~ 1.6°	2, 4, 6, 8, 10	increased by 0.16
	Azimuth, $\phi_1$	0 ~ 360°	3, 6, 9, 12, 15	increased by 360°/Sample Count
Camera	Elevation, $\Theta_2$	54 ~ 90°	2, 4, 6, 8, 10	increased by 0.16
	Azimuth, $\phi_2$	0 ~ 360°	3, 6, 9, 12, 15	increased by 360°/Sample Count
	FOV	90° (fixed)	-	-
ROI	ROI ratio, $\sigma$	1.0 ~ 1.4	1, 2, 3	increased by 0.2

• **Crater Classifiers**

A multiclass SVM classifier, LunarSVM\_ex, was trained using supervised learning and a stochastic gradient solver. Unlike CNN, SVM cannot automatically acquire image features through learning. Therefore, it is necessary to select an appropriate feature and convert it to a pre-prepared composite image. HOG [18] is a typical feature detector that is suitable for images such as craters. However, the prior results showed that the performance of HOG is less than 30%. Therefore we exploit the activation feature of CNNs [19] for LunarSVM\_ex and rely on the fully connected layer of LunarNet\_ex to generate suitable features.

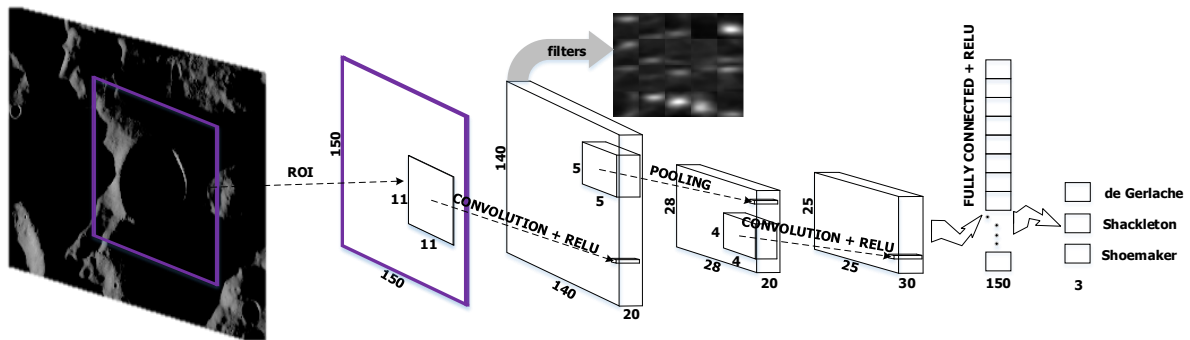


Figure 5: LunarNet\_ex Architecture

LunarNet\_ex consists of 9 layers as shown in Fig. 5 with a relatively shallow CNN as CONVOLUTION (CONV1), Rectified Linear Unit (ReLU1), POOLING, CONV2, ReLU2, FULLY CONNECTED (FC1), ReLU3, FC2 and Softmax. The performance can be improved with a deeper design, but the validation accuracy as a stop condition was set to 90% on average when learning the synthetic data used in this experiment. Rather than designing optimal CNNs, the feasibility of the synthetic data and the closed-loop learning system using it was examined.

In Fig. 5, the input image of 150 x 150 is determined by considering the average size of the ROI, and the stride of the filter of CONV1 is set to 1 to use as much information as possible. It is designed to remove the following POOLING layer after CONV2 and preserve as much information as possible. The final number of classes are three, corresponding to the three craters via a loss function.

• **RESULT**

The performance of LunarSVM\_ex using the activation feature of a specific layer of LunarSVM\_ex did not seem to be better in all cases, but it is generally high. The mean difference in accuracy was not significantly different from LunarNet\_ex.

Intuitively, the performance can be expected to be improved by increasing the sampling frequency of parameters. The test results as shown in Fig. 6 clearly show that performance increases with higher Sun elevation angles (Sun elevation sampling frequency is increased proportionally with elevation angle). It can be guessed that as the Sun elevation increases, more area is illuminated, increasing the information available to classify craters. However, in the case of ROI of 1.4, accuracy decreases as sampling frequency increases as shown in Fig. 6 on top left. We presume that this is due to increasing ROI while the input image resolution remains fixed at 150 by 150. Also, ROI 1.0 sized test data such as shown in Fig. 7 accounted for the largest portion of the total.

Performance does not increase proportionately with increasing sample frequency for Sun azimuth. We observe this because azimuth sampling is done uniformly between 0-360 degrees, and the test data do not contain enough useful information (i.e., were almost completely black) at certain azimuth angles.

Varying the camera elevation sampling frequency does not result in a marked improvement in performance. An average improvement of 5% by increasing the number of training samples from 2,250 to 20,250. LRO, and SELENE cameras were mainly pointed at the nadir direction, which may explain why training lower elevations does not increase accuracy.

Varying camera azimuth generally results in better performance, but the signal is not monotonically increasing and appears to be correlated to camera elevation. The interpretation of this result requires further research. Nevertheless, in the algorithm of Fig. 3, only the Sun Elevation is changed in the machine learning process through the closed loop, which means that the user can set the desired threshold to about 85% as a test accuracy.

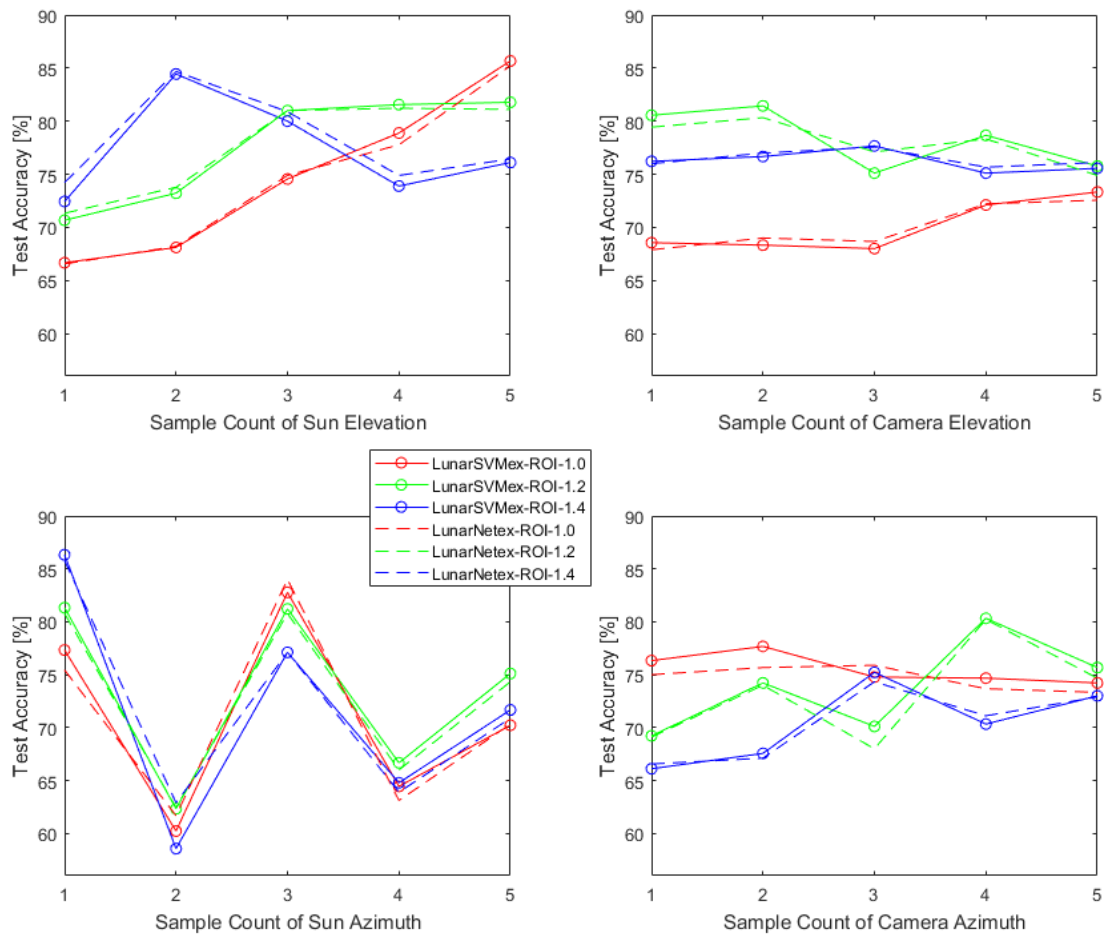


**Figure 6: Test Accuracy by Test Conditions**

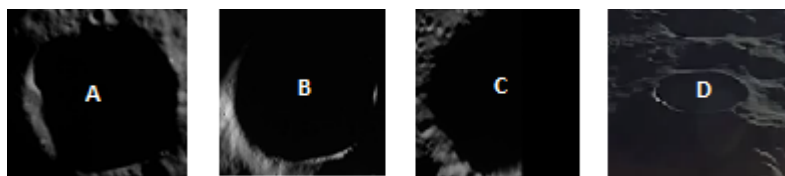


**Figure 7: Test Data with ROI 1.0 and Slewing: A (de Gerlache from TC1W2B0\_01\_00582S883E2719), B (Shackleton from M101457600MC\_pyr), C (Shoemaker from M139810920MC\_py) and D (Shackleton from SELENE HDTV)**



• **DISCUSSION**

The validity of the parameters was examined without finding their optimal values. The possibility of training a dark region classifier was demonstrated using synthetic images infinitely obtained by finely manipulating the parameters in the closed loop algorithm. However, increasing the number of the synthetic data could result in unnecessary time consuming rather than improving performance. We have confirmed that there are still many limitations in evaluating its performance using small amounts of real images with respect to their multiformity. Finally, there is a need to look further at the unexpected result by the parameter, Camera azimuth.

**REFERENCES**

1. M. Yu, H. Cui, Y. Tian; 2014; "A new approach based on crater detection and matching for visual navigation in planetary landing", *Advances in Space Research*; **53**; pp. 1810 - 1821
2. H. Kaufmann, M. Lingenauber, T. Bodenmueller, M. Suppa; 2015; "Shadow-Based Matching for Precise and Robust Absolute Self-Localization during Lunar Landings"; *IEEE Aerospace Conference*, Big Sky, MT, USA; 7-14 March 2015
3. D. Meng, C. Yunfeng, W. Qingxizn, 2013, "Novel approach of crater detection by crater candidate region selection and matrix-pattern-oriented least squares support vector machine", *Chinese Journal of Aeronautics*; **26**;(2); pp. 385 – 393
4. C. Cortes and V. Vapnik, 1995, "Support-Vector Networks", *Machine Learning*, **20**;(3); pp. 273-297
5. Y. LeCun, Y. Bengio, G. Hinton, 2015, "Deep learning". *Nature*, **521**;(7553), pp. 436-444
6. L.F. Palafoxa, C.W. Hamiltona, S.P. Scheidta, A.M. Alvarezb; 2017; "Automated detection of geological landforms on Mars using Convolutional Neural Networks"; *Computers & Geosciences*; **101**; pp. 48 - 56
7. J.P. Cohen, H.Z. Lo, T. Lu, W. Ding; 2016; "Crater Detection via Convolutional Neural Networks"; *47<sup>th</sup> LPSC, Lunar and Planetary Science Conference*; Texas, USA; 21-25 March 2016
8. E. Emami, G. Bebis, A. Nefian, T. Fong; 2015; "Automatic Crater Detection Using Convex Grouping and Convolutional Neural Networks"; *International Symposium on Visual Computing Conference*; Nevada, USA; 14-16 December 2015
9. S.C. Wong, A. Gatt, V. Stamatescu, D. McDonnell; 2016; "Understanding data augmentation for classification: when to warp?"; *DICTA, Digital Image Computing: Techniques and Applications Conference*; Queensland, Australia; 30 November-2 December 2016
10. A. Shrivastava, T. Pfister, O. Tuzel, J. Susskind, W. Wang, R. Webb; 2016; "Learning from Simulated and Unsupervised Images through Adversarial Training"; arXiv:1612.07828
11. A. Boukercha, A. Al-Tameemi, A. Grumpe, C. Wohler; 2014; "Automatic Crater Recognition Using Machine Learning with Different Features and their Combination", *45<sup>th</sup> LPSC, Lunar and Planetary Science Conference*; Texas, USA; 17-21 March 2014
12. NASA; 2017;"PDS Geosciences Node – LOLA Data Node"; <http://pds-geosciences.wustl.edu/missions/lro/lola.htm>
13. M. Kato, S. Sasaki, Y. Takizawa, Kaguya Project Team, 2010, "The Kaguya Mission Overview", *Space Sci Rev*, **154**;(3); pp. 3-19
14. L. Williams, 1978, "Casting Curved Shadows on Curved Surfaces", *Computer Graphics (Proceedings of ACM SIGGRAPH 78)*, pp. 270-274
15. H.H. Lee, D.W. Jung; 2017;"Construction of Validation Bench for Testing of Vision-Based Navigation Methods in the Korean Lunar Exploration Program"; *SESP(Simulation and EGSE for Space Programmes)*; **1**; Noordwijk, Netherlands; 28-30 Mar;
16. H.H. Lee, G. H. Ju; 2014;"A Study on Real Measurement Data based Lunar Virtual Surface Generation"; *KSAS Autumn Conference* ; **1**; Jeju, Korea; 19-21 Nov;
17. STAR-Dundee;"PANGU – Planet and Asteroid Natural scene Generation Utility"; <https://www.star-dundee.com>
18. N. Dalal, B. Triggs; 2005; "Histograms of Oriented Gradients for Human Detection"; *IEEE Computer Vision and Pattern Recognition Conference*; **1**;pp. 886-893
19. J. Donahue, Y. Jia, O. Vinyals, J. Hoffman, N. Zhang, E. Tzeng, T. Darrell; 2013;"Decaf: A deep convolutional activation feature for generic visual recognition"; arXiv:1310.1531